Bima Journal of Science and Technology, Vol. 9(1B) Apr, 2025 ISSN: 2536-6041

DOI: 10.56892/bima.v9i1B.1265

Integrated Geophysical Technique for Characterization of Sedimentary Aquifers of Ankpa, Part of Northern Anambra Basin, Nigeria

Akpah, Fabian A; Musa, Kizito O.*; Shuaibu A. M.; Akudo, Ernest O.; Ahmed II, Jamilu B.; Shaibu, Mary M.; Nanfa, Andrew C.; Jimoh, Jacob B.; Oyedokun Tayo, O.; Fashipe, Winnies B.; Ochogwu Theophilus O.

Department of Geology, Federal University Lokoja, PMB 1154, Kogi State, Nigeria

Corresponding Author: kizito.musa@fulokoja.edu.ng

ABSTRACT

This research focused on addressing the need for potable water supply in semi - rural communities through effective groundwater exploration. The study concentrates on the Ankpa Area, within the Northern Anambra Basin in North Central Nigeria. To achieve this, a combined approach utilizing Geomagnetic Very Low-Frequency Electromagnetic (VLF-EM) and Vertical Electrical Sounding (VES) methods were employed. Forty-five (45) locations were subjected to geophysical survey using the DDR3 Terrameter for VES measurements and the ADMT 300 VLF-EM machine. The VES method, employing Schlumberger electrode configuration, was used to investigate variations in subsurface resistivity within depths ranging from 1 to 200 meters. The collected field data underwent meticulous processing and analysis via WinResist software, resulting in a 1D graph that depicts variations in subsurface layer resistivity. The VLF-EM method was applied to map electromagnetic field variations attributable to shifts in geological formations and groundwater presence. By utilizing the ADMT 300 VLF-EM machine, comprehensive data collection across the study area enabled the creation of a 2D subsurface graph. The integration of these two distinct methodologies culminated in a holistic understanding of subsurface structure, significantly enhancing the precision of potential groundwater-bearing zone identification. The outcomes of the study divulged the presence of 5 to 6 geoelectric layers, encompassing topsoil, lateritic soil, clay, sandstone, and shale. These layers exhibited resistivity values spanning from 42.6 Ωm to 100,000.0 Ωm with an average resistivity value of 10352.25Ωm, accompanied by thickness measurements ranging from approximately 0.5 meters to 93.2 meters with an average thickness of 34 meters. The integrated use of VLF-EM and VES methods in the investigation has revealed the potential for groundwater exploration in the study area average to slightly high.

Keywords: Resistivity, subsurface structure, aquifer zones, groundwater investigation

INTRODUCTION

Water is a vital resource for life, existing in both surface and groundwater forms (Philip *et al.,* 2022, Okoro, *et al.,* 2010). Due to its widespread use in urbanization, industrial growth, and domestic consumption, groundwater is now considered an essential source of water and is thought to be free of contamination (Ojo *et al.,* 2015; Agbasi and Etuk, 2016; Hasan *et al.,* 2018; Shuaibu, 2024). Groundwater exploration is becoming more significant due to the increased demand for water, especially in regions where surface water is limited as a result of climate variability (Alabi *et al.,* 2016).

Its scarcity is a major concern, particularly for the people of Ankpa area, Northern Anambra Basin, during the dry season. Groundwater is essential to life and essential to development for home, industrial, and agricultural uses (Onomohanran, 2013; Shishaye and Nagari, 2016; Adagunodo *et al.,* 2018a). Surface water

DOI: 10.56892/bima.v9i1B.1265

has traditionally provided the majority of the water needed for residential use. However, surface water's capacity has reached its limit as a result of issues including population expansion, climate change, and pollution from human activity (Opara *et al.,* 2020; Urom *et al.,* 2021).

Increased water consumption, limited access to piped water, surface water shortages and contamination are further effects of the spike in rural-to-urban migration. In light of these, groundwater continues to be the main source of supply of clean drinking water for people (Oladejo *et al.,* 2013; Adagunodo, 2018a; Kalaivanan *et al.,* 2019). In view of new issues like diminishing aquifer reserves and the consequences of climate change, this emphasizes the critical need for well-thought-out policies and plans for managing groundwater resources strategically (Barbieri *et al.,* 2021). As a result, the use, measurement, and appraisal of groundwater by means of geophysical and hydrogeological techniques are now of greater importance.

Groundwater exploration has shown success with a variety of geophysical techniques, such as electromagnetic surveys, magnetic studies, electrical resistivity, seismic refraction, magnetotellurics, and gravity measurements. To attain good outcomes, these strategies can be used singly or in combination (Anomohanran and Orhiunu, 2018; Olaseeni *et al.,* 2018; Olaojo *et al.,* 2018; Oyeyemi *et al.,* 2018; Obasi *et al.,* 2021).

The electrical resistivity technique, that is, the vertical electrical sounding (VES) method using the Schlumberger array has become the most widely used geophysical method for groundwater exploration among the previously mentioned approaches (Imam and Hassan, 2019; Kizito *et al.,* 2021).

Its popularity can be ascribed to its simple field operation, data analysis simplicity (Sunmonu *et al.,* 2018), and efficacy in figuring out the resistivity and thickness of different subsurface conducting layers (Egbai et al., 2019). The electrical resistivity method was the mainstay of most of the literature that has been written about groundwater potential in the study region. Unfortunately, this method has not been able to offer a thorough understanding of the groundwater potential, subsurface resistivity distribution, or hydraulic conductivity especially in areas where water yield has been consistently low. But what sets this study apart is its integrated methodology, which combines hydrogeological and geological approaches with geophysical tools (VES and VLF-EM) to assess groundwater potential in detail. The research area's water table depth has been estimated and zones with high groundwater potential have been effectively identified using this methodology.

Location of the Study Area

Ankpa is situated in the northern part of the Anambra sedimentary basin in Nigeria, which has a distinctive funnel-shaped configuration (Figure 1). It is located between latitudes 7º38' N and 7º48' N and longitudes 7.58ºE and 7.66ºE, the Anambra Basin is bordered to the east by the Lower Benue Trough, North by the Bida Basin and South by the Niger Delta Basin. The geological, the Ankpa area is part of the the Anambra Basin which began with the Mid-Santonian deformation in the Benue Trough, shifting the primary deposition area westward and resulting in the basin's formation (Obaje, 2009).

The Ajali Formation, primarily known for its significance in the stratigraphic framework of the Anambra Basin, is a prominent sedimentary unit of Late Cretaceous age (Maastrichtian). The basin, located in southeastern Nigeria, represents a synclinal sedimentary structure that formed due to subsidence during the Santonian tectonic

Bima Journal of Science and Technology, Vol. 9(1B) Apr, 2025 ISSN: 2536-6041
DOI: 10.56892/bima.v9i1B.1265

episode. This basin is filled with a sequence of marine to fluvial deposits, including the Ajali Formation, which reflects a predominantly fluvial depositional environment Obi and Okogbue (2004).

The Ajali Formation is characterized by its coarse-grained, poorly sorted, cross-bedded sandstone with occasional conglomeratic horizons. These sandstones are dominantly quartzose, indicating a high degree of maturity (Ladipo, 1988). The formation is often referred to as "false-bedded sandstone" due to its characteristic large-scale cross-bedding. In some areas, the Ajali Formation also exhibits ironstone and clay intercalations, which suggest periodic changes in depositional energy and conditions (Nwajide, 2013).

The sedimentological attributes of the Ajali Formation point to a braided river system as the primary depositional environment. This is evidenced by:

Large-scale trough cross-bedding, indicative of high-energy water flow.

Absence of marine fossils, suggesting terrestrial deposition.

Vertical stacking patterns typical of fluvial deposits, with periodic exposure and reworking.

Regionally, the Ajali Formation underlies the Nsukka Formation and overlies the Mamu Formation, forming part of the Maastrichtian succession in the Anambra Basin. Its thickness varies, with estimates ranging between 30 and 150 meters depending on the locality, influenced by subsidence and sediment supply rates during deposition (Reijers *et al.,* 2021).

The Ajali sandstones are highly porous and permeable, making them potential aquifers and reservoirs for hydrocarbons. Additionally, the high quartz content of the sandstones is of interest for industrial applications such as glass manufacturing.

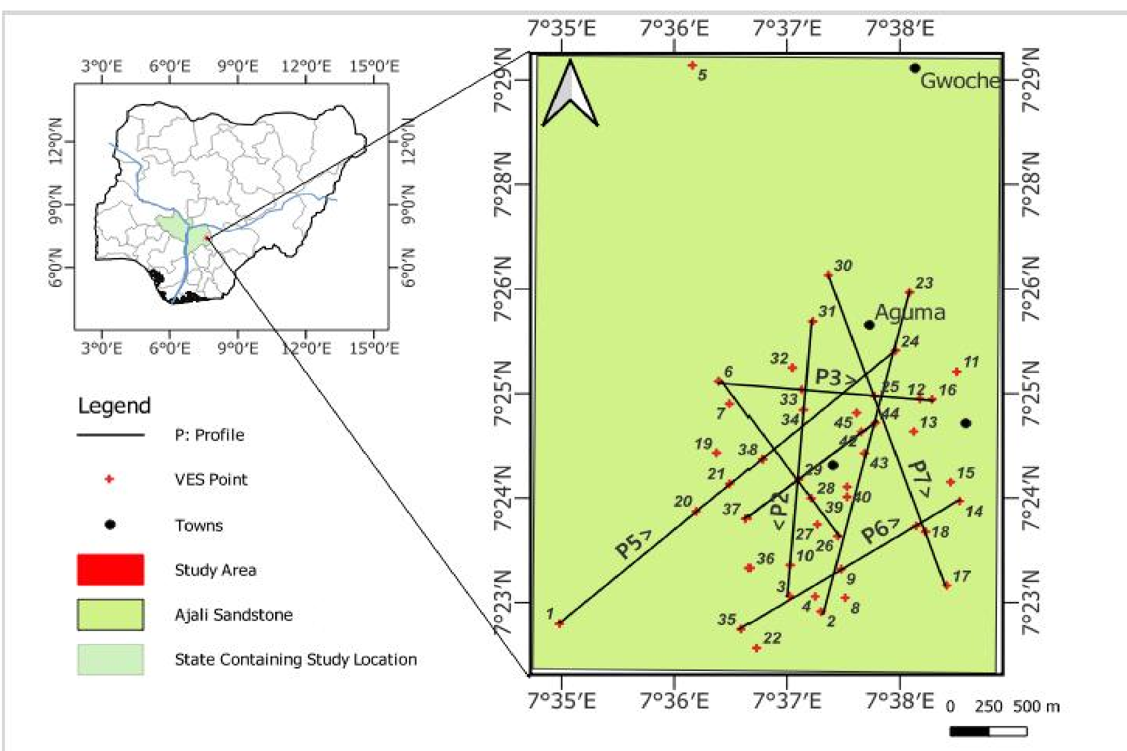

Figure 1: Geological map of Nigeria showing the northern Anambra Basin.

DOI: 10.56892/bima.v9i1B.1265

MATERIALS AND METHODS

Data Acquisition

The Vertical electrical sounding method conducted in the study area was done using Schlumberger electrode array for the data acquisition (Figure 1). DDR3 Sensor Terrameter., utilizing an AB separation of 200 meters. AB/2 ranged from 1 meter to 100 meters. The potential electrode separation P1/P2 varied from 0.2 volts to 8 volts. Four electrodes: two current electrodes denoted as A and B, alongside two potential electrodes labeled as M and N, arranged linearly on the surface, four reels of Cables, Direct Current Source (12 Volts Car battery), hammers, field Survey Data sheet, global positioning system (GPS) and measuring tapes were all used for data acquisition.

Eight profiles lines were selected across the VES points in order to properly delineate the aquiferous units and their thickness/depth (Figures 2, 3, and 4).

Resistivity soundings were performed at forty-five (45) different locations, The Schlumberger electrode configuration adheres to the condition that the distance between the external (current) electrodes (a) is equal to or greater than five times the distance between the potential electrodes (b) (i.e., a≥5b), as noted by previous authors (Philip *et al.,* 2022, Okoro*, et al.,* 2010). Vertical electrical soundings utilizing the Schlumberger array were conducted by maintaining the electrode arrangement centered over a designated field station.

The terrameter readings were noted in the V/l (R) column, which would later be multiplied by a constant K to derive the apparent resistivity values (ρa). All apparent resistivity values were converted to ohm-meters. The AB/2, representing half of the current electrode spacing, and MN/2, indicating half of the potential electrode separation. For the quantitative interpretation of electrical sounding curves, several methods were employed. These methods could be categorized into analytical (computer-based) and manual interpretation approaches.

From Ohm's law which is stated numerically as:

$$V \propto R \tag{1}$$

$$V = IR \tag{2}$$

Where

V = electrical potential,

I = current and

R = resistance to the flow of current.

Direct current (D.C.) was passed into the ground through two electrodes (current electrodes) in order to employ the electrical resistivity method. The potential difference (ΔV) that results from the current flow was then measured through two electrodes (potential electrodes). Figure 3 shows a schematic representation of the relationship between subsurface current and field data gathering.

The depth of investigation, which is a function of electrode spacing, determines how well the current is sensed. The deeper the electric current flows in the earth, the wider the distance between the outer current electrodes; therefore, the deeper the research (Philip et al., 2022; Keary and Brooks, 1991). The kind of rock, fluid quantity, and fluid's hydrogeochemical component all have a significant impact on the ground responses.

The resistivity of a rock material whose resistance is R and having a cross sectional area A and length L is expressed as:

$$\rho = \frac{AR}{L} \tag{3}$$

where,

Bima Journal of Science and Technology, Vol. 9(1B) Apr, 2025 ISSN: 2536-6041
DOI: 10.56892/bima.v9i1B.1265

A= cross-sectional area

R = the resistance measured between two equipotential surfaces;

L = distance separating the two equipotential surfaces.

Aquifer Parameters

According to Singh (2005), the hydraulic properties of aquifers are crucial for the safe building of engineering structures as well as for the evaluation of contaminated land and groundwater. It takes a lot of time and money to estimate aquifer parameters using the field hydrogeological method. As an alternative, the surface geophysical method might offer quick and efficient ways to assess aquifers and explore for groundwater. Geo-electric sections representing the thickness and resistivity of subsurface electrical layers were created by processing the resistivity values (Dahlin et al., 2007).

Aquifer depth and hydraulic conductivity are two of the essential characteristics that define and describe subsurface hydrology. To estimate the spatial distribution of hydraulic parameters, a variety of inquiry methodologies are frequently used.

Field estimations of these parameters are always available and surface resistivity parameters extracted from surface electrical measurements can be highly effective not only for aquifer hydraulic conductivity estimation but also for group of hydraulic parameters. Correlation between hydraulic and electrical aquifer properties can be possible, as both properties are related to the pore space structure and heterogeneity of the medium under study.

Using Dar Zarrouk model, when dealing with a series of horizontally aligned, uniformly consistent, and equally anisotropic layers characterized by resistivity (ρ) and thickness (h), the Dar Zarrouk parameters, namely, the longitudinal conductance (S) and the transverse resistance (T), can be precisely defined as follows:

- H/ρ_n = Longitudinal Conductance (LC), ……………………………………..(4)
- $H*\rho_n$ = Transverse Resistance (TR),………………………………………… (5)
- $386.40\ \rho_n^{-0.93283}$ = Hydraulic Conductivity (HC),…………………………… (6)
- $K*H$ = Transmissivity (T),……………………………………………………(7)
- $\dfrac{\rho_n - \rho_{n-1}}{\rho_n + \rho_{n-1}}$ = Reflection Co-efficient (RC),……………………………………(8)
- $\dfrac{\rho_n}{\rho_{n-1}}$ = Fractured Contrast (FC)……………………………………………..(9)

The Dar Zarrouk parameters in the research area were determined using factors such as the resistivity (ρn) of the nth layer and the resistivity (ρn-1) of the layer immediately above it. These parameters were calculated based on characteristics like the thickness of weathered layers, resistivity of the overlying material, transverse resistance (T), reflection coefficient (RC), formation resistivity (ρ2), and resistivity contrast (FC). Various values for these formation parameters were obtained (Ekwe *et al.,* 2006).

Hydraulic conductivity

Hydraulic conductivity is symbolically represented as *K*, which is a property of rock that describes the ease with which water can move through pore spaces or fractures

(Soupios *et al.,* 2007). It depends on the intrinsic permeability of the material and on the degree of saturation. Saturated hydraulic conductivity, *Ksat*, describes water movement through saturated media.

$K_c = 1/p$ (10)

where Kc is the calculated hydraulic conductivity, and *p* is the resistivity of the saturated layer from VES.

Transmissivity

Transmissivity is a measure of how much water can be transmitted horizontally. It is directly proportional to the hydraulic conductivity (K) and aquifer thickness (b). Expressing K in m/day or cm/s and b in m, the transmissivity (T) measure in m^2/day or cm^2/s.

$T = Kb$ (11)

The transmissivity (T) of aquifer is related to the field hydraulic conductivity (K) by equation 11.

Transmissivity in porous medium is given by;

$T_C = K_C b$ (12)

Where;

T_C = Calculated transmissivity (m^2/day) from VES data.

K_C = Calculated hydraulic conductivity (m/day) from VES data.

b = Thickness of saturated layer (m)

RESULTS AND DISCUSSION

Plotting and modeling was done using the obtained resistivity values for the corresponding VES locations, as indicated by the corresponding graphs, which also included inferred lithologies, depths, thickness, and apparent resistivities (Table 1). The research area's varied subsurface lithofacies were indicated by the geo-electric correlation of the forty- five (45) VES locations. In the research area, there are two (2) to five (5) different geoeletrical layers.

The functionality of the borehole and other factors are significantly impacted by thickness and depth in addition to the apparent resistivity parameter. Aquiferous unit thickness, subsurface stratigraphic successions, presence of impermeable layers, previous geodynamics (such as tectonic and magmatic events where applicable), and variations in geo-thermal and geo-structural occurrences are the main causes of recorded variations in aquifer depths across locations. Consequently, the thickness, depth, and apparent resistivities of the underlying geo-electric layers determine the aquiferous zone's boundary (Table 1). The initial geo-electric layers, that is the top soils, are primarily laterites rich in sand content, clay, shaley and sandstone elements. They have an average apparent resistivities of 876.33 Ωm, 19.44 Ωm and 62.70 Ωm respectively.

The thickness and depth ranges from 0.293 m to 4.193 m with an average 0.820 m (See Table 2). Clay, sandstone, shale, clayey shale, sandy shale, consolidated sandstone and/or saturated sandstone are the seven (7) interlayering geo-electric layers that were discovered in the region. The layers exhibited apparent resistivity values spanning from 10.7 Ωm to 100,000.0 Ωm with an average apparent resistivity value of 8118.58 Ωm, accompanied by thickness measurements ranging from approximately 0.4m to 102m with an average thickness of 23.995m and depth ranging from 0.4m to 198.2m with an average of 49.512m (Table 1).

The following VES curve types were identified in the studied region: K, H, A, AK, KH, HA, and KQ. The most common sounding curve type in the research area is the KA curve type, which is followed by the K curve type (Table 4 and Fig 4). The variety of

Bima Journal of Science and Technology, Vol. 9(1B) Apr, 2025 ISSN: 2536-6041

DOI: 10.56892/bima.v9i1B.1265

curve types supports the area's subsurface litho-unit heterogeneity.
The summary of the average, minimum and maximum apparent resistivity, thickness and depth as presented in Table 1, show case troubling lithofacies (Aquicludes and Aquifuge) relative to groundwater accumulation following their porosity and permeability.

The studied area is generally indicated to be underlain by heterolytic units/formations by the geo-electric layers thickness, depth, apparent resistivity, and inferred lithologies (Table 1). Additionally, several of the VES points in the study indicate that the thickness nature of the aquifer units has a detrimental impact on the groundwater development of the area.

Table 1: Summary of VES Geoelectric Layer Parameters.

VES No.	Resistivity (ohm-m)	Thickness (m)	Depth (m)	Lithology	Curve Type
1.	156.4	2.6	2.6	Sandy shale	A
	7147.6	4.5	7.1	Consolidated Sandstone	
	12892.2	7.8	14.9	Sandstone	
	26443.8	57.8	72.7	Sandstone	
	8065.5	-	-	Dry sandstone	
2.	399.1	1.8	1.8	Top soil	A
	1282.6	26.3	28.1	Sandy shale	
	1739.2	12.2	40.2	Sandstone	
	2776.8	33.4	73.7	Sandstone	
	664.6	49.4	123.1	Shale	
	519	-	-	Saturated sandstone	
3.	396	1.3	1.3	Top soil	KH
	61104.7	16	17.3	Sandstone	
	35099.6	16.3	33.6	Sandstone	
	15761	48.7	82.3	Sandstone	
	10889.2	62.7	145	Consolidated sandstone	
	14736.1			Dry sandstone	
4.	242.9	0.4	0.4	Top soil	KH
	14609.8	9.1	9.5	Sandstone	
	4110	38.9	48.4	Saturated sandstone	
	11782.8	36	84.4	Sandstone	
	829.2	83.8	168.2	Sandy Shale	
	3680	-	-	Sandstone	
5.	201.2	2.1	2.1	Top soil	H
	82.2	8.1	10.1	Clay	
	619.2	5.4	15.5	Sandy Clay	
	1041.1	4.7	20.2	Shale	
	100000			Dry sandstone	
6.	297.7	1.9	1.9	Top soil	KH

Bima Journal of Science and Technology, Vol. 9(1B) Apr, 2025 ISSN: 2536-6041

DOI: 10.56892/bima.v9i1B.1265

	11465.6	8.3	10.3	Sandstone	
	3228.5	21.1	31.3	Sandy Shale	
	15494.3	23.9	55.2	Sandstone	
	57068.1			Sandy sandstone	
7.	397.9	3.7	3.7	Top soil	AK
	13197.6	14.4	18.1	Sandstone	
	16549.2	47.8	65.9	Sandstone	
	7832	48.3	141.2	Consolidated sandstone	
	8586.6			Dry sandstone	
8.	599.5	8.5	8.5	Lateritic Top soil	H
	25.4	15.8	24.4	Clay	
	1753.6	102	126.3	Sandy Shale	
	167.4	41.6	167.9	Sandy Clay	
	466.6			Saturated sandstone	
9.	94.3	3.7	3.7	Top soil	K
	875.3	13.4	17.1	Sandy/Shale	
	122.5	31.5	48.7	Clay	
	943.2	42.5	91.1	Sandy/ shale	
	427.8	25.5	116.7	Shale	
	1412.2	-	-	Saturated sandstone	
10.	264.4	0.5	0.5	Lateritic Topsoil	AK
	3692.7	10	10.4	Sandstone	
	24990.5	30.2	40.7	Sandstone	
	1027.7	76	116.7	Sandy clay	
	984.3	-	-	Saturated sandstone	
11.	312.3	6.2	6.2	Top soil	KH
	2766.7	37.1	43.2	Sandstone	
	286.7	77.3	120.5	Shale	
	10118.9	32.2	152.7	Sandstone	
	940.8	40.1	192.8	Sandstone	
	957			Saturated Sandstone	
12.	337.1	0.5	0.5	Top soil	AK
	4546.9	18.9	19.4	Sandstone	
	10392.5	40.2	59.6	Consolidated Sandstone	
	5414	34.5	94.1	Sandstone	
	2908.8			Saturated sandstone	
13.	190.9	2.2	2.2	Top soil	K
	1827.8	25.4	27.5	Sandstone	
	97.7	54.2	81.7	Clay	
	969.1	23.7	105.4	Sandy shale	

DOI: 10.56892/bima.v9i1B.1265

	372.1	25	130.4	Shale	
	1728.3			Saturated sandstone	
14.	194.2	0.4	0.4	Top soil	K
	65268.1	16.5	16.9	Sandstone	
	10330.9	21.7	38.6	Consolidated sandstone	
	6608.7	26.5	65.1	Sandstone	
	3830.8			Saturated sandstone	
15.	1923	2.5	2.5	Lateritic soil	KQ
	16779	25.3	27.8	Consolidated Sandstone	
	2014.8	17.1	44.9	Sandstone	
	1133.1	53.2	98.1	Sandy/shale	
	6428.5			Sandy sandstone	
16.	322.5	0.5	0.5	Topsoil	K
	2462.9	35.8	36.3	Sandstone	
	1049.9	10.1	46.4	Sandy/shale	
	325.6	33.6	80	Shale	
	1051	43.9	123.9	Shale	
	3198.2	-	-	Sandstone	
17.	1534.2	8.5	8.5	Top soil	KA
	7002.4	8.9	17.4	Sandstone	
	21452.1	28.1	45.5	Compacted sandstone	
	6955.9	42.2	87.6	Sandstone	
	2594.9			Sandstone	
18.	192.3	0.5	0.5	Top soil	K
	8946.3	4.4	4.9	Sandstone	
	1225	25.6	30.6	Sandy/Shale	
	5662.6	42.2	72.8	Sandstone	
	1021.2	94.4	167.2	Sandstone	
	2319.6			Sandstone	
19.	300.4	0.5	0.5	Topsoil	K
	16651.5	13.3	13.8	Consolidated sandstone	
	1590.2	5.3	19.1	Sandstone	
	337.2	6.3	25.3	Sandy/shale	
	82.8			Saturated sandstone	
20.	808.9	3.5	3.5	Laterite topsoil	HA
	376.1	9.2	12.6	Shale	
	8883.9	19.2	31.9	Sandstone	
	22661.7	44.1	76	Sandstone	
	4018.4	10.9	86.9	Sandy shale	

DOI: 10.56892/bima.v9i1B.1265

	25976.2			Sandy sandstone	
21.	189.3	0.4	0.4	Top soil	A
	2328.6	20.7	21.1	Sandstone	
	35890.5	32.6	53.7	C/ Sandstone	
	29298.9	32.4	86.1	C/Sandstone	
	19400.1	34.5	120.6	C/ Sandstone	
	23718.2			Dry sandstone	
22.	627.7	7.5	7.5	Top soil	KH
	13366.3	93.2	100.6	C/ Sandstone	
	4589.9	23.2	123.9	Sandstone	
	10119.7	39.3	163.2	Sandstone	
	6579.9	35.1	198.2	Sandstone	
	14296.7			Sandy sandstone	
23.	2137.7	4.3	4.3	Top soil	HK
	813.2	9.3	13.6	Sandy/Shale	
	16320.7	48.2	61.8	Sandstone	
	2901.7	56.6	118.4	Sandstone	
	7037.2			Sandy sandstone	
24.	350.9	0.4	0.4	Top soil	K
	24766.4	5.2	5.6	Consolidated Sandstone	
	3907.4	18	23.6	Sandstone	
	22361.5	57.8	81.4	Sandstone	
	6135.4	50.8	132.3	Sandstone	
	11101			Sandy/sandstone	
25.	472	1.4	1.4	Topsoil	AK
	1041.2	17.2	18.6	Sand / shale	
	11172.9	28.8	47.3	Consolidated Sandstone	
	665	47.1	94.4	Sandy/shale	
	396.7			Saturated sandstone	
26.	329.3	2.9	2.9	Topsoil	K
	1956.8	21.1	24	Sandstone	
	272.7	35.1	59.1	Shale	
	711.3	29.6	88.7	Sandy/Shale	
	2798.8			Sandstone	
27.	296	1.4	1.4	Topsoil	H
	146.2	12.1	13.5	Clay	
	2610.4	11.6	25.1	Sandstone	
	20017.1	71.3	96.4	Consolidated Sandstone	
	4144.1	24.1	120.4	Sandstone	

Bima Journal of Science and Technology, Vol. 9(1B) Apr, 2025 ISSN: 2536-6041
DOI: 10.56892/bima.v9i1B.1265

	16156.3			Sandy/sandstone	
28.	428.6	3.7	3.7	Topsoil	AK
	2612.2	8.7	12.5	Sandstone	
	4787.6	36.6	49.1	Sandstone	
	1819.7	50.7	99.8	Clayey/Sandstone	
	3097.9			Sandstone	
29.	295.5	0.6	0.6	Topsoil	AK
	3314.2	7.1	7.7	Shale	
	38544.2	29.8	37.6	Consolidated Sandstone	
	6436.1	57.5	95.1	Sandstone	
	6321.6	42.1	137.2	Sandstone	
	8441.3			Dry sandstone	
30.	694.3	2.5	2.5	Lateritic Topsoil	AK
	1870.9	13.3	15.8	Sandstone	
	12087.5	36.6	52.4	Consolidated Sandstone	
	4284.1	56.4	108.8	Sandstone	
	3303.6			Sandstone	
31.	183.9	1	1	Topsoil	H
	10.7	5.3	6.3	Clay	
	587.9	26.5	32.7	Shale	
	441.8	20.1	52.8	Shale	
	1887.9			Sandstone	
32.	395.9	2.8	2.8	Topsoil	AK
	12399.5	11.6	14.5	Sandstone	
	34541.1	31.9	46.3	Sandstone	
	12560.8	43.5	89.9	Sandstone	
	5990.9			Sandy/sandstone	
33.	183.3	1.9	1.9	Topsoil	AK
	20880.5	4	5.9	Sandstone	
	46331.7	26.7	32.6	Sandstone	
	5561.8	61.2	93.8	Shale	
	3878.7			Sandstone	
34.	391.4	3.6	3.6	Topsoil	A
	5140.5	11.8	15.4	Shale	
	11866.2	60.7	76.1	Sandstone	
	6412.2	40	116.1	Sandy shale	
	4983.1			Sandstone	
35.	216.5	0.8	0.8	Topsoil	AK
	14900.8	8	8.8	Sandstone	
	56484.4	28.9	37.7	Sandstone	

DOI: 10.56892/bima.v9i1B.1265

	12022.8	36.3	74	sandstone	
	12181.5	28.2	102.2	compacted sandstone	
	7868.6			sandstone	
36.	244.6	0.4	0.4	Topsoil	A
	6831.8	32.3	32.7	Shale	
	13171.7	21.4	54.1	Sandstone	
	27644.3	40.2	94.3	Sandy/shale	
	12094.2	38.5	132.9	Sandstone	
	7447.2			Sandstone	
37.	227.5	0.5	0.5	Topsoil	A
	26743.9	14.2	14.7	Sandstone	
	35157.2	38.3	53	Consolidated sandstone	
	15927.4	49	102	Sandstone	
	14224.3			Sandstone	
38.	42.6	1.3	1.3	Topsoil	A
	3440.8	4.1	5.3	Shale	
	61591.1	37.1	42.4	Sandy shale	
	24953.7	25.3	67.8	Sandstone	
	49817.8			Sandstone	
39.	149.7	1.6	1.6	Topsoil	KH
	1177.1	20.8	22.4	Shale	
	117.3	22.4	44.8	Sandy Clay	
	794.9	15.1	59.9	Sandstone	
	948.7	12.2	72.2	Sandy shale	
	14045.3			Sandstone	
40.	79	1.9	1.9	Topsoil	A
	296.8	13.6	15.6	Clay	
	1145.4	7.5	23.1	Sandy shale	
	2524.2	7.6	30.7	Sandstone	
	100000			Sandstone	
41.	146.4	6.7	6.7	Topsoil	A
	120.2	12.4	19.1	Clay	
	2847.4	13.2	32.4	Shale	
	3386.7	9.6	42	Sandstone	
	5506.1			sandstone	
42.	1062.6	11.3	11.3	Topsoil	KH
	8581.4	19.5	30.7	Sandstone	
	1992.4	31	61.8	Sandy Shale	
	1519.7	38	99.8	Sandstone	
	1839.3	38.4	138.2	Sandstone	

Bima Journal of Science and Technology, Vol. 9(1B) Apr, 2025 ISSN: 2536-6041
DOI: 10.56892/bima.v9i1B.1265

	1602.1			Saturated sandstone	
43.	50.7	1.7	1.7	Topsoil	KH
	3356.2	15.5	17.2	Shale	
	723.6	38.2	55.4	Sandy clay	
	1230.4	46.5	102	Shale	
	1963			Sandstone	
44.	633.8	15.2	15.2	Lateritic top soil	K
	2737.6	16.1	31.3	Sandstone	
	2340.9	29.8	61.1	Sandstone	
	966.1	39.3	100.4	Sandy shale	
	846.1	42.2	142.5	Sandy shale	
	1362.1			Sandstone	
45.	322.5	0.5	0.5	Topsoil	K
	2462.9	35.8	36.3	Sandstone	
	1049.9	10.1	46.4	Sandy shale	
	325.6	33.6	80	Shale	
	1051	43.9	123.9	Sandstone	
	3198.2			Sandstone	

The interpreted VES data indicates that the top geoelectrical layer across the study area ranges from 0.5 to 14.5 m in thickness (Figure 2). The southeastern portion exhibits the greatest average thickness, reaching 10.5 m. The spatial distribution of the shallow aquiferous units (unsaturated zone) shows a thickness varying between 15 and 30 m, with the southern, southeastern, and northeastern extremes displaying the highest values, averaging 20 m (Figure 3).

For the deep aquifer, which ranges from semi-confined to confined conditions, geospatial analysis reveals thicknesses between 10 and 170 m. The southeastern region consistently exhibits the greatest thickness, as depicted in Figure 4.

The geo-electric sections (Figure 5, 6, 7, 8, 9, 10 and 11) as well as aquiferous model and characteristics (Table 1) revealed variations in layer resistivity and thickness both vertically and laterally. The cross section of the geospatial analysis of both the unconfine and confined aquifer were modeled and presented along the geoelectrical sections.

These findings provide insight into the major variability in lateral and vertical lithological alterations within the research area. The geo-electric layer segment revealed three to six subterranean layers, majorly sandstone which is the major aquiferous unit. The profile 1 (Figure 5) shows that the research area aquiferous unit is confined (VES 43 and 43) at depth of 130m above and some area is unconfined (VES 23, 24) this is due to depositional sequence of sedimentary materials from different source.

Bima Journal of Science and Technology, Vol. 9(1B) Apr, 2025 ISSN: 2536-6041
DOI: 10.56892/bima.v9i1B.1265

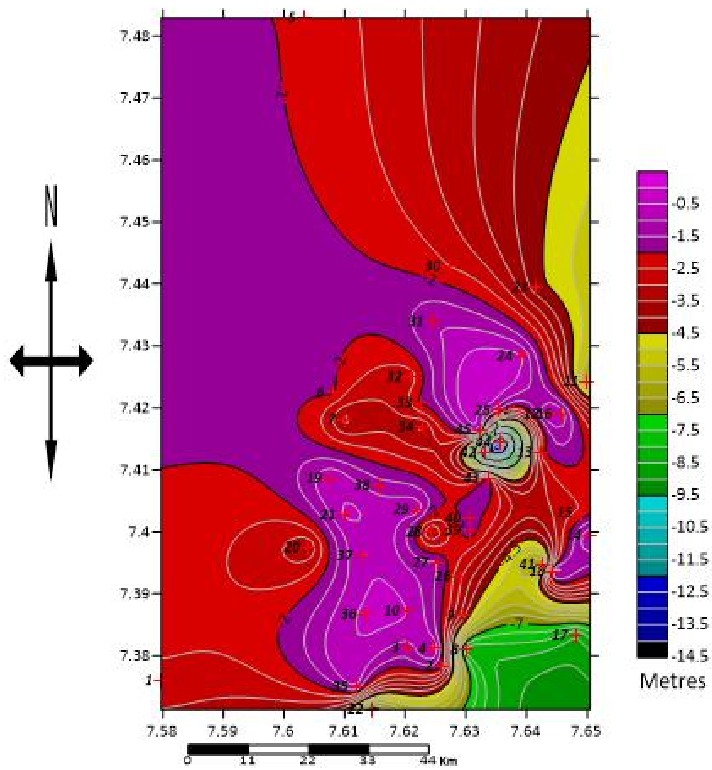

Figure 2: Spatial Distribution of Top Geoelectrical Layer.

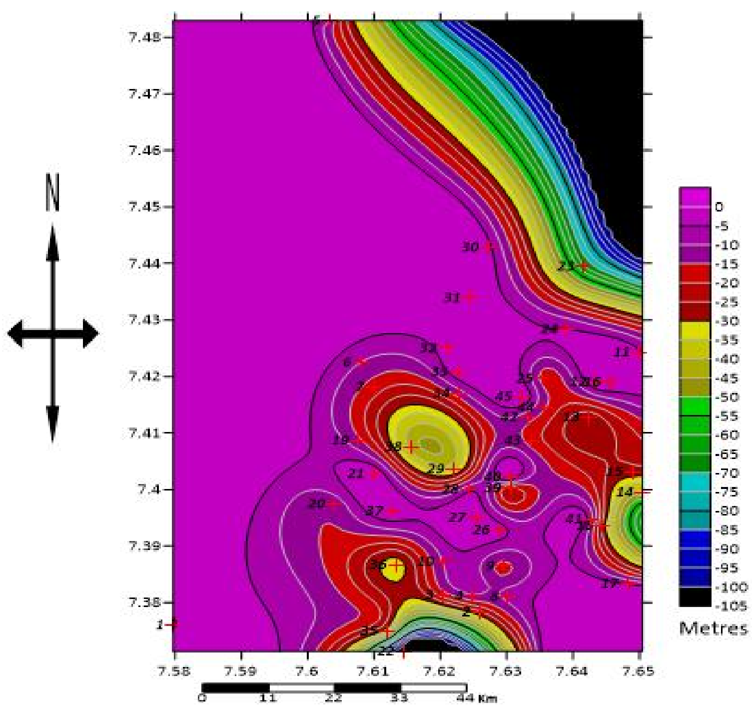

Figure 3: Geospatial Analysis of Shallow Aquiferous Layer.

Bima Journal of Science and Technology, Vol. 9(1B) Apr, 2025 ISSN: 2536-6041
DOI: 10.56892/bima.v9i1B.1265

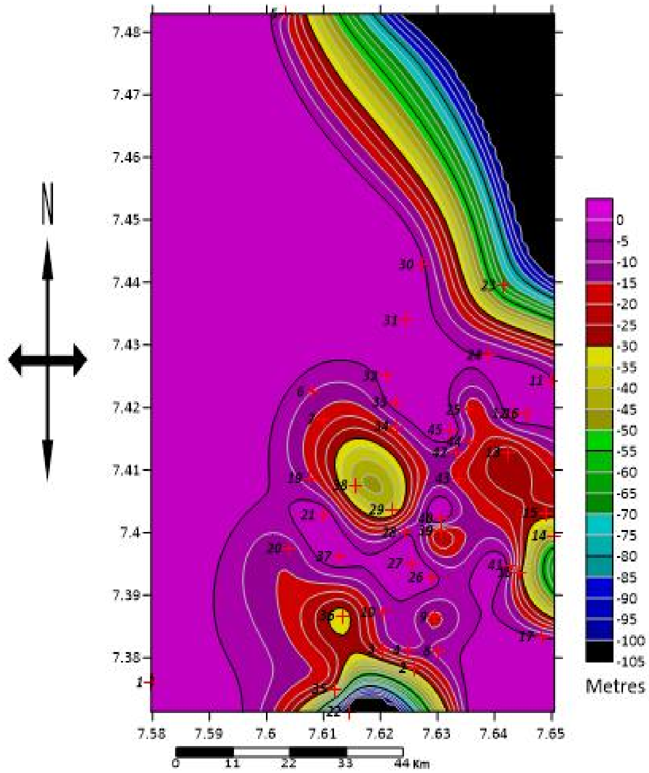

Figure 4: Spatial Analysis of the Deep Aquiferous Layer

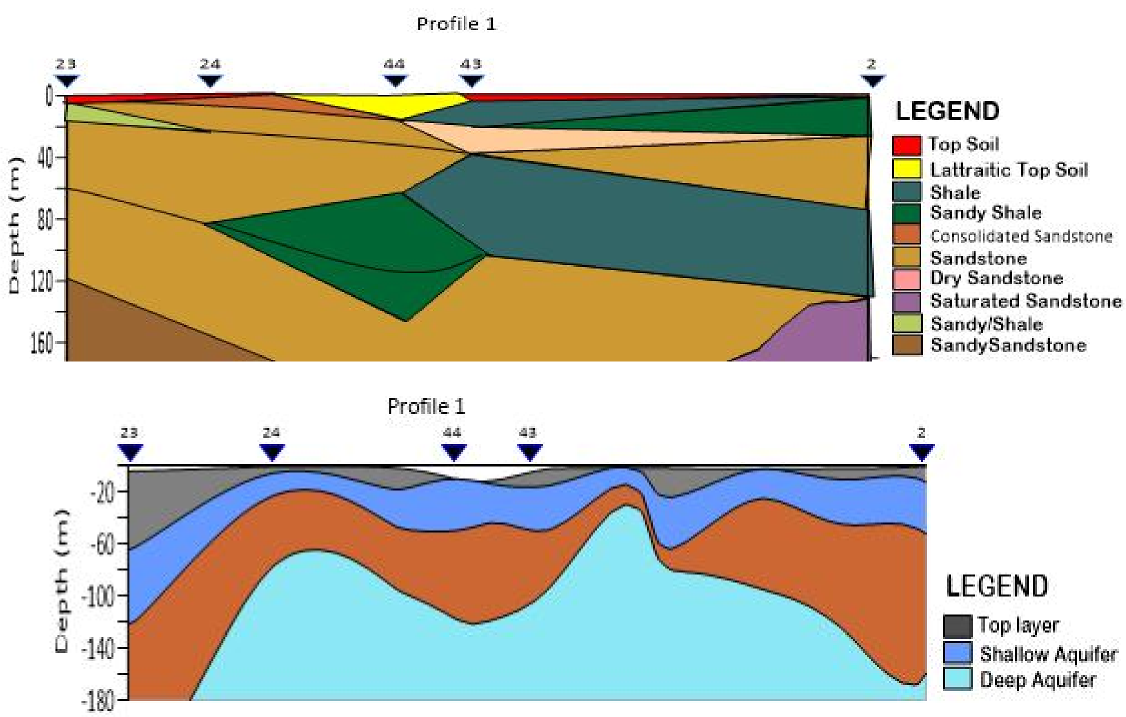

Figure 5: Geoelectrical Section of Profile 1/Aquifers Geometry.

Bima Journal of Science and Technology, Vol. 9(1B) Apr, 2025 ISSN: 2536-6041

DOI: 10.56892/bima.v9i1B.1265

The non-uniformity and contrasting heterogeneous subsurface lithofacies in the area make it challenging to pinpoint a precise depth point for groundwater occurrence (Figure 6), such as VES 2, 3, 10, 15, 16, 28, 29, 38, 39 and 42. Profile 2 shows that VES 31 is confined aquiferous unit with depth of 160m. Whereas, VES 34, 29 depict unconfined/semi-confined aquiferous layer at depth of 100m.

Not every VES point was found to contain a litho-unit with textural features that promote groundwater accumulation and discharge (Figure 7). It is obvious that only VES 6 along this profile may be productive in terms of groundwater development.

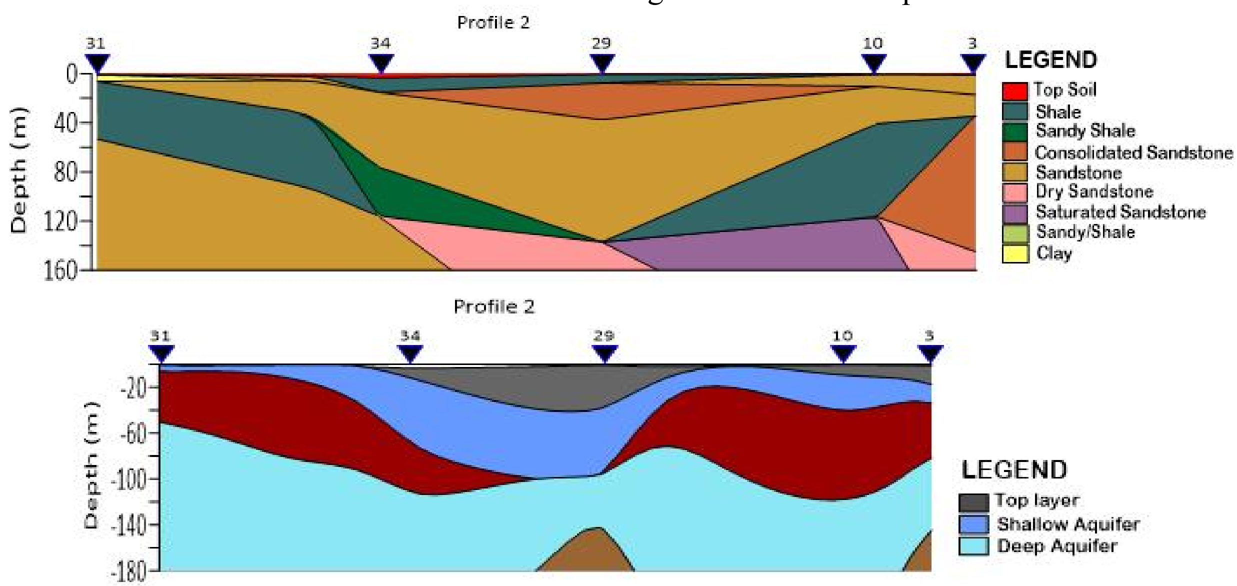

Figure 6: Geoelectrical Section of Profile 2/Aquifer Geometry.

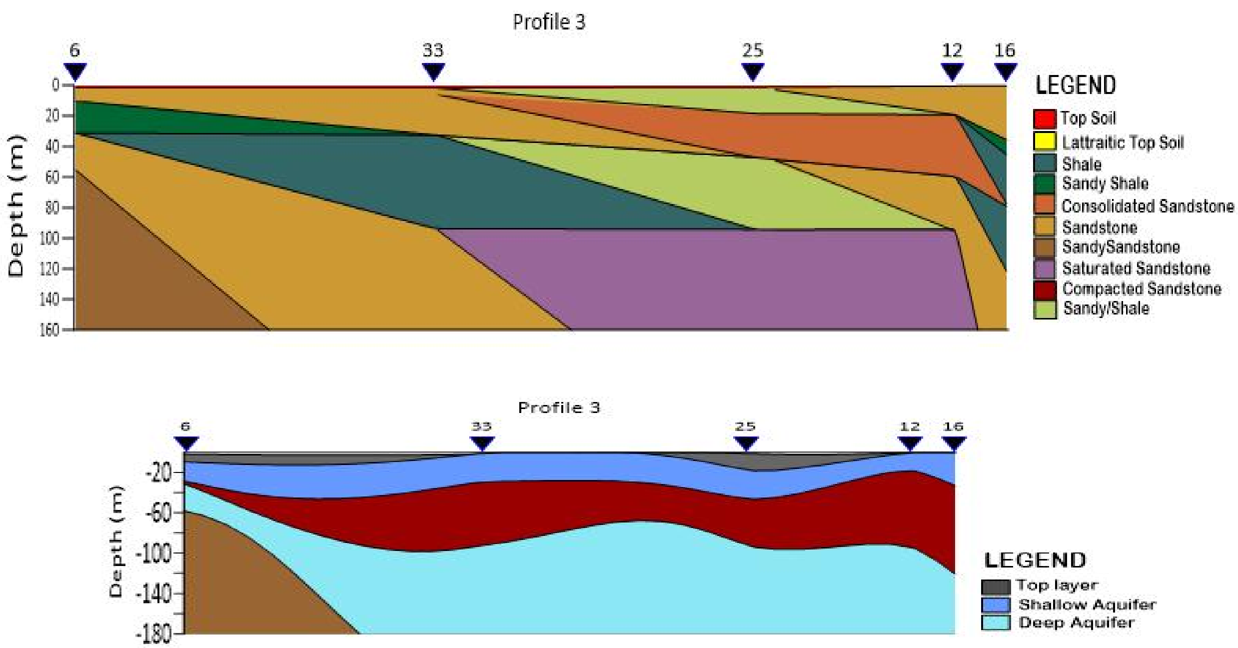

Figure 7: Geoelectrical Section of Profile 3/Aquifer Orientation.

Bima Journal of Science and Technology, Vol. 9(1B) Apr, 2025 ISSN: 2536-6041

DOI: 10.56892/bima.v9i1B.1265

It is highly probable that primary porosity will be quite low in these areas due to the presence and influence of shale litho-facies inside the sandy-shale aquiferous unit (Figure 8), which would result in very poor water transmission and storage. In contrast, the sands typically retain a significant amount of water and create a stable aquifer (Odoh, 2010; Edet et al., 2011).

Profile 5 and 6 (Figures 9 and 10) reveals an alternation of sandstone and shale lenses, while VES 24, 14, 41 and 35 indicates the presence of a confined aquiferous layer with a thickness ranging from 40 to 120 meters. The remaining segments of the profile exhibit aquiclude or aquifuge characteristics, making them unsuitable for groundwater development. Therefore, VES 24, 14 and 41 are the most promising location for groundwater exploration and development.

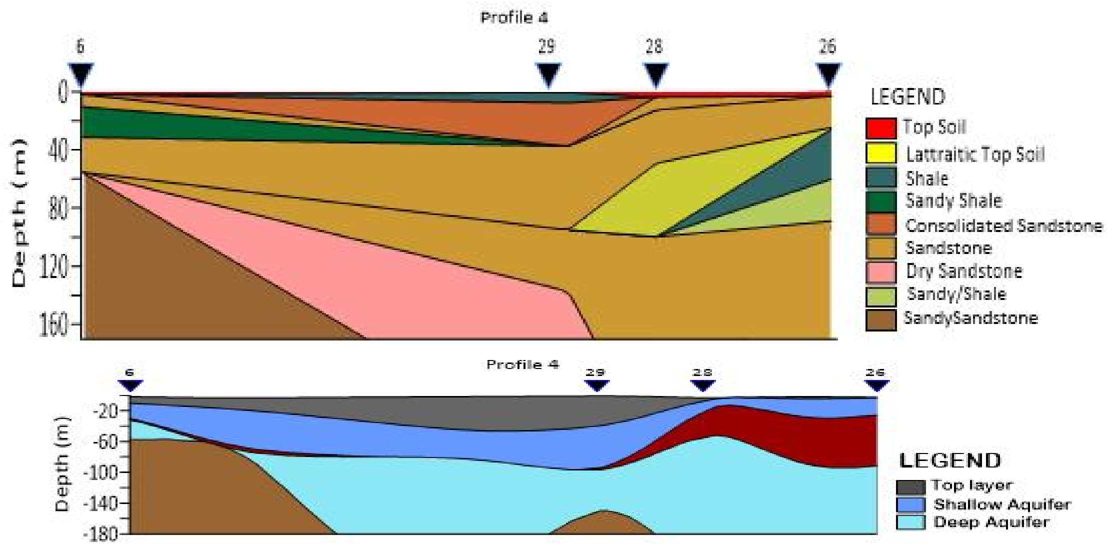

Figure 8: Geoelectrical Section of Profile 4/Aquifer Geometry.

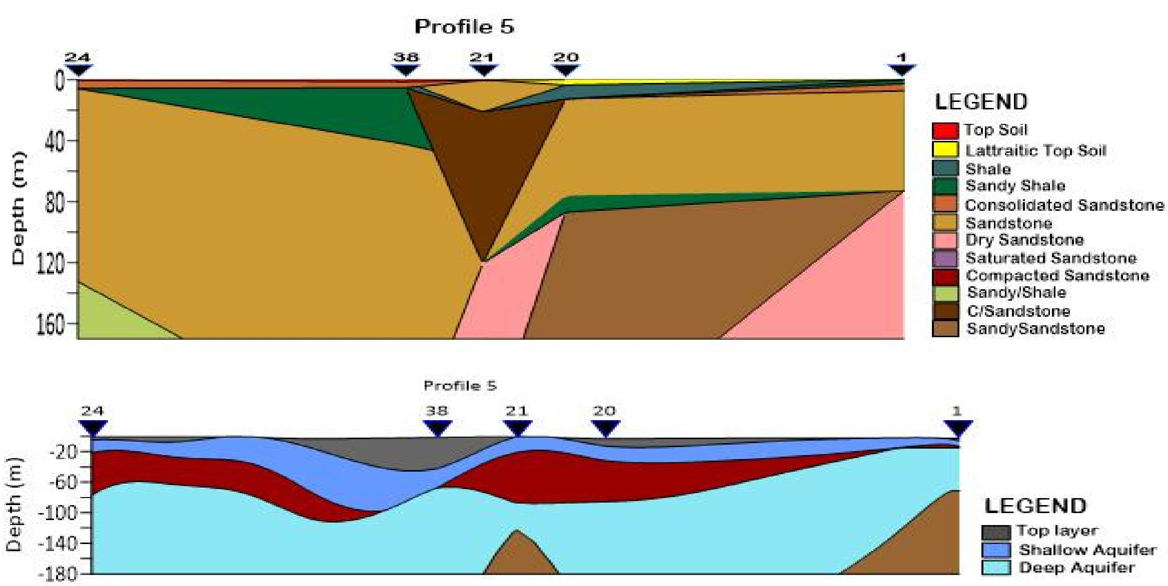

Figure 9: Geoelectrical Section of Profile 5/Aquifer Geometry.

DOI: 10.56892/bima.v9i1B.1265

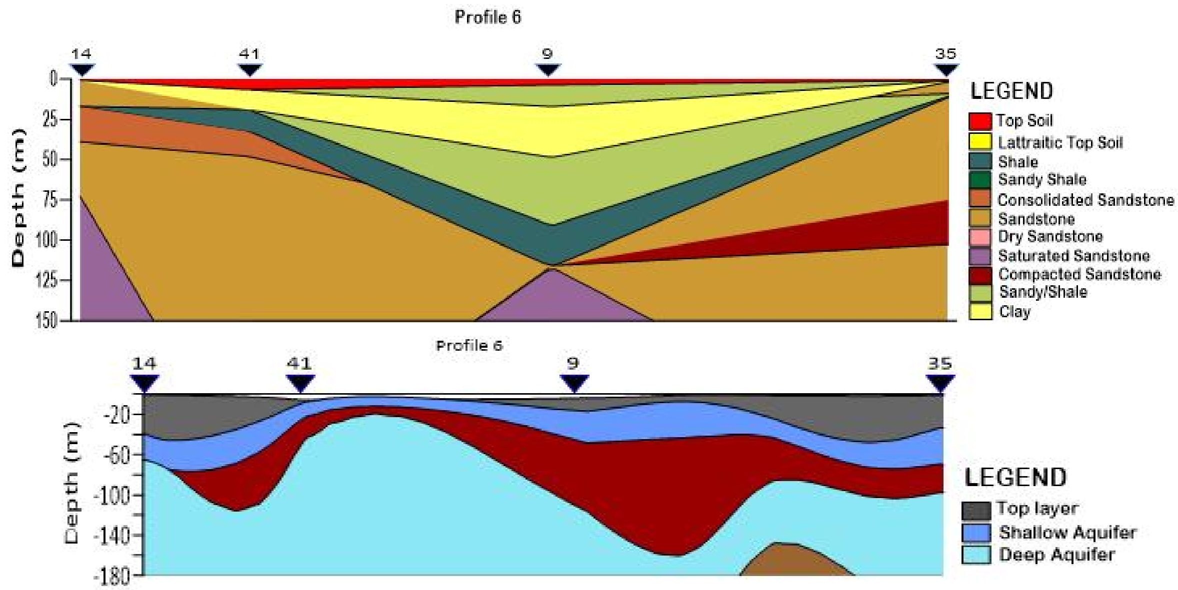

Figure 10: Geoelectrical Section of Profile 6/Aquifer Orientation.

In this sedimentary formation, the alternation of shale and saturated sandstone is a common geological phenomenon. This alternation has significant implications for groundwater flow, as it creates a complex hydrogeological environment.

Shale layers act as aquitards, which are low-permeability units that restrict groundwater flow, (Figure 11) they are typically composed of fine-grained minerals, such as clay and silt, which reduce their permeability. In contrast, saturated sandstone layers serve as aquifers, which are permeable units that store and transmit groundwater. The alternation of shale and sandstone creates a confined aquifer system, recharge occurs through the saturated sandstone layers, while discharge occurs through wells or other aquifer outlets.

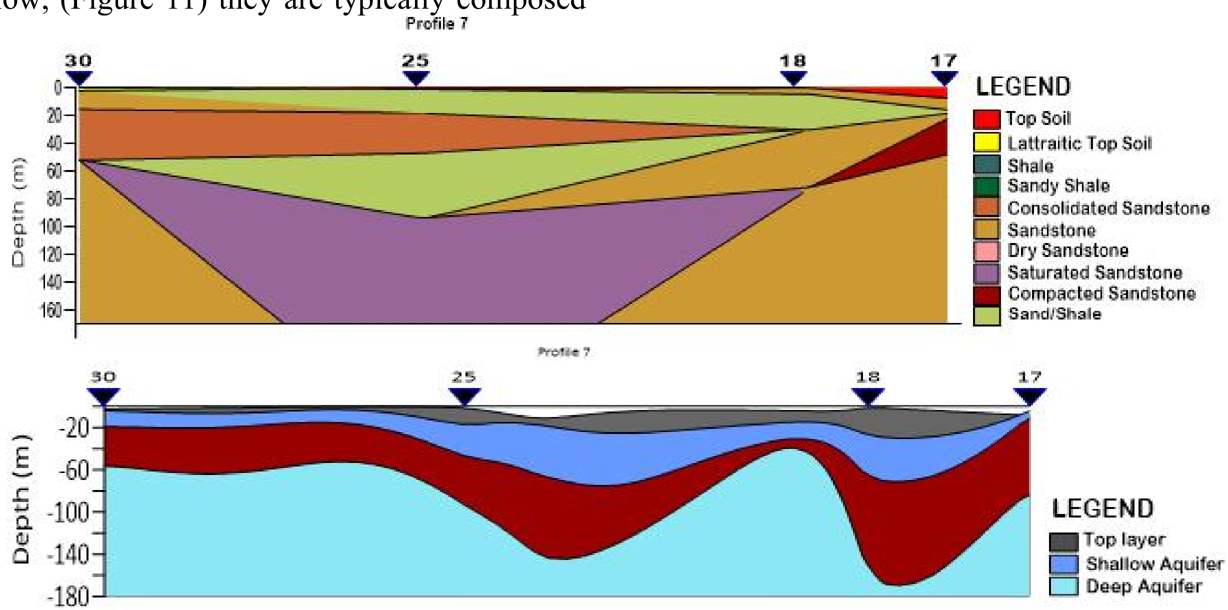

Figure 11: Geoelectrical Section of Profile 7/Aquifer Structure.

DOI: 10.56892/bima.v9i1B.1265

All things considered, the geo-electric model's confinement of the majority of the aquifer units highlights the borehole's possible failure rate even more because the aquifer will only be able to supply base flow.

This suggests that drawdown, head loss, and submersible pump damage will occur at a high echelon and that the probability function of discharge surpassing recharge will be prominent, leading to frequent borehole failure as has been observed in the research area. While remembering that groundwater scarcity undoubtedly ranks first among the causes of borehole failures, it is not the sole contributing factor.

The model highlights the depth at which deep aquifers are located. These aquifers typically represent significant water-bearing formations beneath the surface and are crucial resources for water extraction in areas where shallow aquifers are insufficient.

The top layers of the geoelectrical section are assessed for their thickness, which can indicate overburden material such as soil or less permeable formations lying above aquifers. Variations in thickness can impact the recharge and protection of the underlying aquifers.

Shallow aquifers are identified with their corresponding depth ranges. These are often closer to the surface and might be more susceptible to contamination but are easier to access for water extraction.

The geoelectrical cross-section illustrates how aquifers of varying depths and thickness are distributed within the subsurface. This visual model aids in understanding the spatial distribution and potential yield of the aquifers.

Aquifer Parameters Characterization of the Study Area

The Dar-Zarrouk parameter idea was used to establish the aquifer parameters of the study area. With an average of 5.4×10^{-2} m/day, the aquifer hydraulic conductivity measured in the research region (Table 2) ranges from 3.05×10^{-2} to 3.26×10^{1} m/day. Based on the obtained results, Bear (1972) classified the area as having semi-pervious relative permeability. It also shows that the area is primarily composed of fine-very fine friable sand, and shale, indicating that the aquifer's output and attribute will probably range from good to bad in terms of water outflow.

The lithology features may have had an impact on a porous rock's hydraulic conductivity, which varies depending on the volume (thickness), arrangement, and textural qualities of the layer as well as the amount of fluid it contains as shown the model (Figures 6, 7, 8). The indirect and direct aquifer characterization in this case will be greatly influenced by the mineral content (mostly clay minerals) and pore size distributions.

The aquiferous zone has an apparent resistivity contrast that varies from 167.4 Ωm to 24953.7 Ωm, with an average of 4819.6 Ωm. These units, which range in degree of fluid saturation from saturated fine sand, medium, to extremely coarse sand, are indicated in the geoelectrical model of subsurface layers and apparent resistivity contouring (Table 2, Figures 6 to 12) characteristic of aquifer materials. Given that the pore fluid and the grain matrix both conduct electrical current, the change in conductivity of these saturated zones could be caused by the different concentrations of dissolved contaminants, high water resistivities, and tiny grain sizes (Iduma *et al.,* 2016; Krasny, 1993).

The average value of the aquifer transmissivity is 2.01×10^{1} m^2/day, with a range of 7.7×10^{-1}

Bima Journal of Science and Technology, Vol. 9(1B) Apr, 2025 ISSN: 2536-6041

DOI: 10.56892/bima.v9i1B.1265

to 13.54X10^1 m^2/day (Table 2). The confined character of the majority of the aquifers and the minimum depth of the aquifer unit in the area (20 m) increase the likelihood of borehole failures, particularly when the aquifer thickness is below 4.7m. In comparison, the average aquifer depth is 105.3m, with variations ranging from 20.2m to 198.2m and thickness from 4.7m to 94.4m with an average of 39.40m. Since the thickness of the shallow aquifer(s) is/are modest, a borehole has a significant probability of failing in such a scenario. The depth range suggests the occurrence of both shallow and deep aquifer in the area. With an average of 185589.5Ω2m throughout the region, the transverse resistance varies from 4893.17Ω2m to 780442.6Ω2m (Table 2).

Table 2: Estimated Aquifer Parameters of the Study Area

VES NO.	LC	TR	HC	T	RC	FC
1.	0.01	466	0.09	5.06	-0.53	0.30
2.	0.07	328	0.89	44.44	-0.61	0.23
3.	0.01	682	0.06	4.15	-0.18	0.69
4.	0.10	695	0.73	61.32	-0.86	0.07
5.	0.01	489	0.59	2.78	0.25	1.68
6.	0.01	370	0.05	1.13	0.65	4.79
7.	0.01	378	0.09	4.35	-0.35	0.47
8.	0.25	696	3.25	135.43	-0.82	0.09
9.	0.06	109	1.36	34.60	-0.37	0.45
10.	0.07	781	0.59	45.52	-0.92	0.04
11.	0.04	377	0.65	26.08	-0.82	0.09
12.	0.01	186	0.13	4.38	-0.31	0.52
13.	0.07	930	1.5	38.63	-0.44	0.38
14.	0.004	175	0.11	2.79	-0.21	0.63
15.	0.05	603	0.54	29.09	-0.28	0.56
16.	0.10	109	1.75	58.81	-0.52	0.31
17.	0.006	293	0.10	4.24	-0.51	0.32
18.	0.09	964	0.60	56.88	-0.09	0.83
19.	0.05	549	1.69	27.61	-0.65	0.21
20.	0.003	438	0.16	1.83	-0.69	0.17
21.	0.002	669	0.04	1.33	-0.20	0.66
22.	0.005	231	0.11	3.72	-0.21	0.65
23.	0.02	164	0.23	12.87	-0.69	0.17
24.	0.01	312	0.11	5.74	-0.59	0.27
25.	0.07	313	0.89	42.34	-0.88	0.06

26.	0.04	211	0.84	24.99	0.44	2.61
27.	0.005	999	0.16	3.93	-0.65	0.21
28.	0.03	923	0.35	17.82	-0.44	0.38
29.	0.006	266	0.11	4.63	-0.01	0.98
30.	0.01	242	0.16	8.92	-0.47	0.35
31.	0.05	888	1.3	26.46	-0.14	0.75
32.	0.01	260	0.12	5.03	-0.70	0.17
33.	0.01	340	0.12	7.58	-0.78	0.12
34.	0.006	256	0.11	4.34	-0.29	0.54
35.	0.004	222	0.09	2.52	-0.20	0.65
36.	0.003	466	0.06	2.31	-0.39	0.43
37.	0.003	780	0.04	2.27	-0.37	0.45
38.	0.001	631	0.03	0.77	-0.42	0.40
39.	0.01	116	0.64	7.87	0.08	1.19
40.	0.003	191	0.25	1.96	0.37	2.20
41.	0.003	325	0.19	1.89	0.08	1.18
42.	0.02	703	0.34	13.29	0.09	1.21
43.	0.04	572	0.51	23.55	0.25	1.70
44.	0.05	357	0.72	30.30	-0.06	0.87
45.	0.10	109	1.80	58.46	-0.52	0.31
Min	0.001	109	0.03	0.77	-0.09	0.04
Max	0.25	780	3.25	135.43	0.65	4.79
Mean	0.03	186	0.54	20.09	-0.33	0.69

LC = Longitudinal conductance, TR = Transverse Unit Resistance, HC = Hydraulic Conductivity, T = Transmissivity, RC = Reflection Coefficient, FC = Fracture Contrast.

Table 3(a-c) presents an overview of the groundwater supply and productive potential in the research region, together with protective capacity rating, transmissivity, and percentage area coverage. These data have been changed based on specific requirements.

Table 3a: Characterization of Aquifer Transmissivity Potentials of the area (after Standard of Krasny, 1993).

Transmissivity Rate	Transmissivity Potentials	VES Locations	Percentage (%)
> 500	High Potential	Nil	0
50 – 500	Medium Potential	4, 8, 16, 18& 45	11.11
5 – 50	Low Potential	1,2,9,10,11,13,15,19,23,24,25,26, 28,30,31,32,33,39,42,43&44	46.67
0.5 – 5	Very Low Potential	3,5,6,7,12,14,17,20,21,22,27,29,3 4,35,36,37,38,40&41	42.22
< 0.5	Negligible	Nil	

Bima Journal of Science and Technology, Vol. 9(1B) Apr, 2025 ISSN: 2536-6041
DOI: 10.56892/bima.v9i1B.1265

Table 3b: Aquifer Transmissivity and Longitudinal Conductance Standard for Groundwater Characterization (Modified Aquifer Transmissivity Standard Gheorghe, 1978).

Transmissivity (m^2/day)	Designation	Groundwater Supply potential	VES Location	Percentage (%)
>1000	Very High	Withdrawal of great regional importance	Nil	Nil
100 -1000	High	Withdrawal of lesser regional importance	8	2.22
10 – 100	Intermediate	Withdrawal of local water supply (small Communities)	2,4,9,10,11,13,15,16,18,19,23,25,26,28,31,42,43,44,&45	42.22
1 – 10	Low	Smaller withdrawal for local water supply (private Consumption)	1,3,5,6,7,12,14,17,20,21,22,24,27,29,30,32,33,34,35,36,37,39,40 &41	53.33
0.1 – 1	Very Low	Withdrawal for local water supply with limited Consumption	38	2.22
< 0.1	Impermeable	Source for Local water supply is difficult, if possible, to ensure	Nil	Nil

Table 3c: Modified Aquifer Productive Capacity Rating (Modified after Oladapo and Akintorinwa, 2007)

Longitudinal conductance (Ωm)	Protective Capacity Rating	VES Locations	Percentage (%)
>10	Excellent	Nil	Nil
5 – 10	Very Good	Nil	Nil
0.7 – 4.9	Good	Nil	Nil
0.2 – 0.69	Moderate	8	2.22
0.1 – 0.19	Weak	4,16&45	6.67
< 0.1	Poor	1,2,3,5,6,7,9,10,11,12,13,14,15,1718,19,20,21,22,23,24,25,26,27,28,29,30,31,32,33,34,35,36,37,38,39,40,41,42,43&44	91.11

CONCLUSION

This research successfully employed an integrated geophysical approach, utilizing Very Low-Frequency Electromagnetic (VLF-EM) and Vertical Electrical Sounding (VES) methods, to characterize the groundwater potential in the Ogaji Community within the Ankpa region of the Anambra Basin, Nigeria. The study identified significant variations in resistivity, depth, and thickness across five to six geoelectric layers, including topsoil, clay, sandstone, and shale. These findings revealed both shallow and deep aquifers with varied hydraulic properties.

The results highlight the heterogeneity of the subsurface lithology, which poses challenges to groundwater exploration and borehole sustainability. Despite this, the integrated geophysical techniques demonstrated high precision in identifying promising groundwater-bearing zones, suggesting that future water resource management strategies could be enhanced using such approaches.

The study underscores the importance of detailed geophysical investigations to address groundwater scarcity, mitigate borehole failures, and ensure sustainable water supply in regions with complex geological formations. The methodologies and findings provide a valuable framework for groundwater exploration in similar sedimentary formations.

REFERENCES

Adagunodo, T. A., Akinloye, M. K., Sunmonu, L. A., Aizebeokhai, A. P., Oyeyemi, K. D., & Abodunrin, F. O. (2018). Groundwater exploration in Aaba residential area of Akure, Nigeria. *Frontiers in Earth Science*, *6*, 66.

Agbasi, O. E., & Etuk, S. E. (2016). Hydro-geoelectric study of aquifer potential in parts of Ikot Abasi Local Government Area, Akwa Ibom State using electrical resistivity soundings. *Int J Geol Earth Sci*, *2*(4), 43-54.

Alabi, O. O., Ojo, A. O., & Akinpelu, D. F. (2016). Geophysical investigation for groundwater potential and aquifer protective capacity around Osun State University (UNIOSUN) College of Health Sciences. *American Journal of Water Resources*, *4*(6), 137-143.

Anomohanran O. (2013). Geophysical Investigation of Groundwater Potential in Ukelegbe, Nigeria. Journal of Applied Sciences, 13 (1), 119-125.

Anomohanran, O. and Orhiunu, M.E. (2018) Assessment of Groundwater Occurrence in Olomoro, Nigeria Using Borehole Logging and Electrical Resistivity Methods. *Arabian Journal of Geoscience s*, 11, 1-9. https://doi.org/10.1007/s12517-018-3582-7

Barbieri, M., Franchini, S., Barberio, M. D., Billi, A., Boschetti, T., Giansante, L., ... & Stockmann, G. (2021). Changes in groundwater trace element concentrations before seismic and volcanic activities in Iceland during 2010–2018. *Science of the Total Environment*, *793*, 148635.

Bear J (1972) Dynamics of fluids in porous media. Elsevier, New York.

Dahlin, T., Wisén, R., & Zhang, D. (2007). 3D effects on 2D resistivity imaging–modelling and field surveying results. In *Near Surface 2007-13th EAGE European Meeting of Environmental and Engineering Geophysics* (pp. cp-30). European Association of Geoscientists & Engineers.

Edet, A.E., Nganje, T.N., Ukpong, A.J., et al., 2011. Groundwater chemistry and quality of Nigeria: A Status Review. African Journal of Environmental Science and Technology. 5(13), 1152-1169.

Egbai, J. C., Oseji, J. O., Ogala, J. E., & Emmanuel, E. D. (2019). Resistivity method applied to aquifer protection study in Agbor-Obi and environs, Delta State, Nigeria. *International Journal of Applied Engineering Research*, *14*(2), 373-383.

Ekwe, A. C., Onu, N. N., & Onuoha, K. M. (2006). Estimation of aquifer hydraulic characteristics from electrical sounding data: the case of middle Imo River basin aquifers, south-eastern Nigeria. *Journal of spatial hydrology*, *6*(2).

Gheorghe, A. (1978). Processing and Synthesis of Hydrogeological Data. Abacus Press, Tumbridge wells, Kent.

Hasan, M., Shang, Y., Akhter, G., & Jin, W. (2018). Delineation of saline-water intrusion using surface geoelectrical method in Jahanian Area, Pakistan. *Water*, *10*(11), 1548.

Iduma, R.E.O., Abam, T.K.S., Uko, E.D. (2016). Dar Zarrouk Parameter as a Tool for Evaluation of Well Locations in Afikpo and Ohaozara, Southeastern Nigeria. Journal of Water Resource and Protection. 8, 505-521.

Imam, A., & Hassan, Q. (2019). Geophysical investigation for groundwater potential of an area in Delhi NCR. *Jordan Journal of Civil Engineering*, *13*(2).

DOI: 10.56892/bima.v9i1B.1265

Kalaivanan, K., Gurugnanam, B., Suresh, M., Kom, K. P., & Kumaravel, S. (2019). Geoelectrical resistivity investigation for hydrogeology conditions and groundwater potential zone mapping of Kodavanar sub-basin, southern India. *Sustainable Water Resources Management*, *5*, 1281-1301.

Keary, P. and Brooks, M. (1991) An Introduction to Geophysical Exploration. 2nd Edition, Blackwell Scientific Publications, Oxford, 254 pp.

Kizito O. M., Adama, B.O. & Ahmed II, J.B (2021): Effects of Solid Waste Disposal on the Groundwater Resources of Okene and Environs, Kogi State, North Central Nigeria; *Water Resources Journal of Nigerian Association of the Hydrogeologists, NAH, Vol 31, Number 1, pp 1-14.*

Krasny, J. (1993). Classification of Transmissivity Magnitude and Variation. Groundwater 31(2), 230-236.

Ladipo, K. O. (1988). Depositional environment and tectonic significance of the Ajali Sandstone in the Anambra Basin. *Journal of African Earth Sciences,* 7(5-6), 819-828.

Nwajide, C.S (2013) Geology of Nigeria's sedimentary basins. CSS Bookshops Limited, Lagos, p 565.

Obaje N. G. (2009). Geology and Mineral Resources of Nigeria. Springer Dordrecht Heidelberg London New York, 23-36.

Obasi, P.N., Eyankware, M.O., Akudinobi, B.E.B. (2021). Characterization and evaluation of the effects of mine discharges on surface water resources for irrigation: a case study of the Enyigba Mining District, Southeast Nigeria. Applied Water Science. 11, 112. DOI: https://doi.org/10.1007/s13201-021-01400-w

Obi C.G and Okogbue C.O (2004) Sedimentary response to tectonism in the Campanian–Maastrichtian succession, Anambra Basin, Southeastern Nigeria. J Afr Earth Sci 38:99–108.

Odoh, B.I., 2010. Surface-outcrop characterization for fracture flow of groundwater: case study of ABakaliki Basin, Ebonyi State, Nigeria. International Archive of Applied Sciences & Technology. 1(1), 45- 53.

Ojo, J. S., Olorunfemi, M. O., Akintorinwa, O. J., Bayode, S., Omosuyi, G. O., & Akinluyi, F. O. (2015). GIS integrated geomorphological, geological and geoelectrical assessment of the groundwater potential of Akure Metropolis, southwest Nigeria. *J Earth Sci Geotech Eng*, *5*(14), 85-101.

Okoro, E. I., Egboka, B. C. E., Anike, O. L., & Enekwechi, E. K. (2010). Evaluation of Groundwater Potentials in parts of the escarpment areas of southeastern, Nigeria. *International journal of geomatics and geosciences*, *1*(3), 544-551.

Okoro, E. I., Egboka, B. C. E., Anike, O. L., & Enekwechi, E. K. (2010). Evaluation of Groundwater Potentials in parts of the escarpment areas of southeastern, Nigeria. *International journal of geomatics and geosciences*, *1*(3), 544-551.

Oladapo, M.I., Akintorinwa, O.J. (2007). Hydrogeophysical study of Ogbese, southwestern. Niger Global Journal of Pure and Applied Science. 13(1), 55-56.

Olaojo, A.A., Oladunjoye, M.A., Sanuade, O.A. (2018). Geoelectrical assessment of polluted zone by sewage effluent in University of Ibadan campus southwestern Nigeria. Environ. Monit. Assess. 190, 24. https://doi.org/10.1007/s10661-017-6389-1

Olaseeni, O. G., Sanuade, O. A., Adebayo, S. S., & Oladapo, M. I. (2018). Integrated geoelectric and hydrochemical assessment of Ilokun dumpsite, Ado Ekiti, in southwestern Nigeria. *Kuwait Journal of Science*, *45*(4).

Oyeyemi, K.D., Aizebeokhai, A.P., Olofinnade, O.M., Sanuade, O.A. (2018). Geoelectrical investigations for groundwater exploration in crystalline basement terrain, SW Nigeria: implications for groundwater resources sustainability. Int. J. Civ. Eng. Technol. 9 (6), 765–772.

Philip O., Ekinya, A., Akpa, C., & Edene, E. (2022). Characterization of Subsurface Lithology and Aquifer Parameters Using Vertical Electrical Sounding (VES) for Groundwater Development in Igbo-Imabana, Southern Nigeria. *Advances in Geological and Geotechnical Engineering Research*, *4*(3), 12–31. https://doi.org/10.30564/agger.v4i3.4939

Phillips, E., Bergquist, B. A., Chartrand, M. M., Chen, W., Edwards, E. A., Elsner, M., ... & Passeport, E. (2022). Compound specific isotope analysis in hydrogeology. *Journal of Hydrology*, *615*, 128588.

Reijers, T. J. A., Petters, S. W., & Nwajide, C. S. (2021). The Niger Delta Basin. Geology and Petroleum Geology of the Niger Delta. Open Journal of Geology, Vol.11 No.5, May 20, 2021. https://doi.org/10.1016/S1874-5997(97)80010-X.

Shishaye, H. A., & Nagari, A. (2016). Hydrogeochemical Analysis and Evaluation of the Groundwater in the Haramaya Well Field, Eastern Hararghe Zone, Ethiopia. J Hydrogeol Hydrol Eng 5: 4. *of*, *10*, 2.

Shuaibu, A., Kalin, R. M., Phoenix, V., Banda, L. C., & Lawal, I. M. (2024). Hydrogeochemistry and water quality index for groundwater sustainability in the Komadugu-Yobe Basin, Sahel Region. *Water*, *16*(4), 601.

Singh, K. P. (2005). Nonlinear estimation of aquifer parameters from surficial resistivity measurements. *Hydrology and Earth System Sciences Discussions*, *2*(3), 917-938.

Soupios, P. M., Kouli, M., Vallianatos, F., Vafidis, A., & Stavroulakis, G. (2007). Estimation of aquifer hydraulic parameters from surficial geophysical methods: A case study of Keritis Basin in Chania (Crete–Greece). *Journal of Hydrology*, *338*(1-2), 122-131.

Sunmonu, L. A., Adagunodo, T. A., Adeniji, A. A., & Ajani, O. O. (2018). Geoimaging of subsurface fabric in Awgbagba, Southwestern Nigeria using geomagnetic and geoelectrical techniques. Malaysian Journal of Fundamental and Applied Sciences Vol. 14, No. 2 (2018) 312-324. http://dx.doi.org/10.13140/RG.2.2.33399.52642.